Cellular, molecular and biochemical impacts of silver nanoparticles on rat cerebellar cortex

Eman Mohamed
: Zagazig University Faculty of Human Medicine
Asmaa A.A. Kattaia (asmaaalhosiny7@gmail.com)
Zagazig University Faculty of Human Medicine https://orcid.org/0000-0002-7188-0100
Rehab Abdul-Maksoud
Zagazig University Faculty of Human Medicine
Samia Abd El-Baset
Zagazig University Faculty of Human Medicine

Research article

Keywords: Cerebellar cortex, cellular and molecular impacts, Rat, Silver nanoparticles

Posted Date: November 4th, 2020

DOI: https://doi.org/10.21203/rs.3.rs-100800/v1

Version of Record: A version of this preprint was published at Cells on December 22nd, 2020. See the published version at https://doi.org/10.3390/cells10010007.

Abstract

Background The excessive exposure to silver nanoparticles (Ag-NPs) has raised concerns about their possible risks to the human health. The brain is a highly vulnerable organ to nano-silver harmfulness. The aim of the current work was to evaluate the impacts of Ag-NPs exposure on the cerebellar cortex of rats especially changes at the ultrastructural and molecular levels.

Methods Forty adult male albino rats were assigned to: control, vehicle control, Ag-NP-exposed groups (at doses of 10mg and 30mg/kg/day). Cerebellar cortex samples were processed for light and electron microscope examinations. Immunohistochemical localization of c-Jun N-terminal kinase (JNK), nuclear factor kappa beta (NF-κB) and Calbindin D28k (CB) proteins was performed. Tissue homogenates were prepared for analysis of gene expression of DNA damage inducible transcript 4 (Ddit4), flavin containing monooxygenase 2 (FMO2) and thioredoxin-interacting protein (Txnip). Serum levels of inflammatory cytokines interleukin-1 beta (IL-1β), interleukin-6 (IL-6) and tumor necrosis factor-alpha (TNF-α) were also measured.

Results Ag-NPs exposure resulted in activation of apoptosis cascades coupled with stimulation of oxidative stress and inflammation pathways. This was evident by the upregulation of Ddit4 gene expressions and JNK protein immune expressions. Alterations of redox homeostasis were verified by enhancement of Txnip and FMO2 gene expressions, favoring the activation of inflammatory responses by increasing NFκB immune expressions and serum inflammatory mediator levels. Another considerable cytotoxic effect was the reduction of CB immune expressions, the crucial regulator of intracellular calcium level.

Conclusion Ag-NPs exposure provoked biochemical, cellular and molecular changes of rat cerebellar cortex in a dose-dependent manner.

Introduction

The innovation of nanomaterials has evoked advancements in science and engineering researches. Nanomaterials are considered the materials for future owing to their distinctive properties and varied applications. (Ndukwu et al. 2020). Silver nanoparticles (Ag-NPs) are among the most hazardous metal nanoparticles due to the extensive uses and the inevitable exposure of human. They have been widely used in the production of cosmetics, healthcare products and wound dressings. They have antibacterial efficacy and more recently, synergistic effects with antibiotics against resistant bacterial species (Liao et al. 2019). The anti-fungal properties against Candida albicans and the antiviral potentials against SARS-Cov, influenza A/H1N1, HIV, HBV, and encephalitis viruses have been also reported (Patra and Baek 2017; Xiang et al. 2011).

The impact of Ag-NPs depends mainly on the particle size. The smaller particles can induce greater harmfulness due to increased mass diffusivity, attachment efficiency, and deposition velocity of

nanoparticles over the biological or solid surfaces (Liu et al. 2010). However, the shape and solubility of Ag-NPs could also affect the cellular uptake, which in turn influence the cytotoxicity (Stoehr et al. 2011).

Cellular uptake of Ag-NPs occurs via active and passive transport; it includes phagocytosis, endocytosis, diffusion or direct penetration through the ion channel (Haase et al. 2011; Murugan 2015). When Ag-NPs enter cells; they become more toxic than in the environment. Inside cells; nano-silver are converted from the elemental silver (Ag^0), to Ag^+ ions then to silver oxide species (Ag–O–) and lastly to silver sulfide species (Ag–S–) that bind to thiols (Wang et al. 2015). However, in the environment, Ag-NPs enter sulfidation reactions to Ag_2S, which decrease their toxicity (Li et al. 2017).

Nano-silver can be absorbed through different routes as ingestion, injection, inhalation or skin contact. When enter blood stream; it binds to plasma proteins and blood cells to be distributed to all the organs (Wijnhoven et al. 2009). Brain is liable to silver accumulation comparative to other organs (van der Zande et al. 2012). They can reach the brain through the upper respiratory tract and sensory nerves in the olfactory bulb (Oberdörster et al. 2009) or through the blood brain barrier (BBB) by transcytosis of capillary endothelial cells (Tang et al. 2010). They can cross the tight junction of BBB and increase its permeability favoring many other harmful substances to enter the brain (Trickler et al. 2010). Additionally, they can pass through synaptic membrane or neuron cell membrane through the ionic channels for Na^+, K^+, Ca^{2+}, and Cl^- (Yang et al. 2010).

c-Jun N-terminal kinase (JNK) is one of mitogen-activated protein kinases (MAPK); a group of serine-threonine proteins responsible for modulating many cellular responses. Under stress conditions, JNKs stimulate apoptosis by enhancing pro-apoptotic genes or by affecting the actions of pro- and anti-apoptotic proteins of mitochondria (Dhanasekaran and Reddy 2008).

Calbindin D28k (CB) is a calcium-binding protein that plays a neuroprotective role by buffering intracellular Ca^{++}. CB has been involved in integrative functions of the cerebellar cortex (Strick et al., 2009). CB is used as a marker for Purkinje cells in normal and degenerative conditions (Verdes et al., 2010). CB depletion is combined with serious neurological disorders involving motor sensory, cognitive and affective impairments (Barski et al. 2003).

Based on this background, the aim of the current study was to assess the impacts of Ag-NPs exposure on the cerebellar cortex of adult male albino rats especially changes at the ultrastructural and molecular levels. Alterations in JNK, nuclear factor kappa beta (NF-κB) and CB proteins and their influences on cellular degeneration processes were examined. We analyzed recently introduced genes involved in apoptotic and oxidative stress cascades including DNA damage inducible transcript 4 (Ddit4), thioredoxin-interacting protein (Txnip) and flavin containing monooxygenase 2 (FMO2). Serum levels of inflammatory cytokines were also measured. Detection of Ag-NPs was achieved using scanning electron microscopy (SEM) and energy dispersive X-ray (EDX) detector.

Materials And Methods

Chemicals

Silver nanoparticles Ag-NPs (nano powder, CAS-No. 7440-22-4) was obtained from Sigma-Aldrich Chemicals, Cairo, Egypt.
They contain poly vinyl pyrrolidone (PVP) as a dispersant. They have the following properties: purity 99.5% based on Trace Metals Analysis; average hydrodynamic diameter after water dispersion 83 nm (SD 37), D10 45 nm, D50 76 nm based on Nanoparticle Tracking Analysis, formula weight 107.87 g/mole; negative charge with a zeta potential -33 mV, as provided by the supplier.

PVP (CAS-No. 9003-39-8; powder) was obtained from Sigma-Aldrich Chemicals, Cairo, Egypt.

Experimental Animals

Forty Wistar albino rats (adult 7 to 9-week age, male, weighing 200–250 g) were attained from the Animal House of the Faculty of Medicine, Zagazig University, Egypt. We put the animals in plastic cages under normal laboratory conditions with suitable temperature (22 ± 2 °C), humidity (60± 10%) and organized photoperiod of 12 h-dark and 12 h-light. They were allowed free access to food and water. All procedures were done according to institutional guidelines for the use of experimental animals and approved by Institutional Animal Care and Use Committee IACUC (protocol approval number: 6937), Zagazig University, Egypt and conformed to NIH Guidelines for the Care and Use of Laboratory Animals.

Characterization of Ag-NPs

The size and shape of Ag-NPs were inspected using transmission electron microscope (JEOL JEM 1010; Jeol Ltd., Tokyo, Japan). The aqueous dispersion of the nanoparticles was dropped on a carbon- coated copper grid which was dried then examined.

Experimental Procedure

After 1-week acclimation, rats were parted randomly into four groups (10 rats each). Treatments were given by oral gavage for 28 days. Group I (control group) received saline in an equivalent volume to that in Ag-NPs-treated groups. Group II (vehicle control group) received PVP (11.5 mg/mL) (Hadrup et al. 2012). Group III (low-dose group) and group IV (high-dose group) were administered Ag-NPs at concentrations of 10mg and 30mg/kg/day respectively (dissolved in saline solution, gavage volume 10 mL/kg) (Kim et al. 2008; Xu et al. 2015a).

At the end of experiment: rats were injected with intraperitoneal thiopental 50 mg/kg. Cerebellar specimens were cut; parts of them were used for histopathological preparations; and others were frozen immediately and stored at –80 ◦C until preparing tissue homogenates for molecular analysis.

Biochemical and molecular study

Measurement of inflammatory markers

Blood samples were left to clot for 2 hours and then centrifugation was conducted at 1000 xg for 20 min to separate sera which were stored at -20 °c till being used. Assays of serum interleukin-1 beta (IL-1β), interleukin-6 (IL-6) and tumor necrosis factor-alpha (TNF-α) were achieved using commercially available enzyme linked immunosorbent assay (ELISA) kits (R&D Systems, Minneapolis, MN, USA) conferring to manufacturer's guidelines.

RNA extraction and quantitative real time transcription polymerase chain reaction (Real-time PCR)

Extraction of total RNA from the cerebellar tissue was achieved using Trizol reagent (Invitrogen, Carlsbad, CA) according to the instructions of the manufacturer. RNA concentration and purity were estimated using spectrophotometer (a NanoDrop ND-1000, Wilmington, DE) at 260 and 280 nm respectively. Reverse transcription was performed using Superscript II reverse transcriptase kit (Invitrogen, Thermo Fisher Scientific) according to the manufacturer's protocol.

Gene expression analyses of DNA damage inducible transcript 4 (Ddit4), thioredoxin-interacting protein (Txnip) and flavin containing monooxygenase 2 (FMO2) were performed in duplicate using real-time PCR detection system (LightCycler, Roche Diagnostics). Glyceraldehyde-3-phosphate dehydrogenase (GAPDH) was used as a house keeping gene for gene expression normalization. PCR amplification was performed in 20ul reaction mixture containing 1 ul template cDNA, 0.4 mM of each primer, 10ml 2X SYBR green PCR master (Qiagen, Hilden, Germany) and the final volume was adjusted with double distilled water. The sequence of the used primers is listed in (Table 1). The following cycling conditions were used: initially 10 min at 94°C, then 35 cycles of denaturation for 10s at 94°C, annealing, extension for 18s at 72°C and finally at 72°C for 10 min. Melting curves were constructed to ensure amplification of the specified genes. Gene expression of the specified genes was represented as fold change which was calculated by the $2^{\Delta\Delta}$CT method (Livak and Schmittgen 2001).

Table 1 Primers and annealing conditions used for real-time PCR

Gene	5'–3' forward primer	5'–3' reverse primer	Annealing condition
Ddit4	TAACACCAGGGAGCTGC	ACAGTTCACTCCTCCAGTACA	56°C, 9 s
Bhlhb2	GGG AGCAGA GTG GTA GTG AC	TGG TGG GAT GAG ATA GAAGG	56°C, 12 s
Txnip	GGAGAAAGTTCTGCTCTCG	AAGTGCTAAGGCGGAGTAA	56°C, 9 s
FMO2	TCACCTGGAGAAGCCAAC	CGGTGATGGAGAAAAGTG	56°C, 7 s
GAPDH	GTATGTCGTGGAGTCTACTG	TTTAGTGGGCCCTCGGC	58°C, 6 s

Histopathological Study

Scanning electron microscopy (SEM) and energy dispersive X-ray (EDX) detector

Detection of Ag-NPs in the cerebellar cortex of exposure groups was done using SEM (JEOL JSM-6510LV electron microscope; Jeol Ltd, Tokyo, Japan) and EDX detection by X-ray analyzer (X-Max^N 20 SDD system, Oxford Instruments, Oxford, UK). In this technique, a high-resolution image was generated by scanning the prepared sample, and then EDX detector verifies the elemental compositions of the image.

Hematoxylin and Eosin (H&E) study

Specimens for light microscopy were fixed in 10% buffered formalin and processed to prepare 5-µm-thick paraffin sections for H&E stain (Bancroft and Gamble. 2008).

Immunohistochemical Study

Following the manufacturer's instructions, avidin biotin complex (ABC) method (ABC Peroxidase Staining Kits, Code No. 32020, Thermo Scientific, Rockford, USA) is used for immunohistochemical staining of the calcium binding protein Calbindin D28k (CB), the apoptotic marker c-Jun N-terminal kinase (JNK) and the inflammatory marker nuclear factor kappa beta (NF-κB). Removal of wax and hydration of sections of paraffin were the beginning points. Antigen retrieval was performed by using citrate buffer and microwave for 15 minutes. Tissues block was done by bovine serum albumin. Then, sections were incubated with the specific primary antibody overnight (4 ◦C): anti-CbD28k (rabbit polyclonal antibody; Cat. #PA5-85669; dilution 1/500; Thermo Scientific, CA, USA), anti-JNK antibody (rabbit polyclonal antibody; code No. ab112501; dilution 1/100; Abcam, Cambridge, UK) and anti-NF-κB (rabbit polyclonal antibody; Cat. #RB-9034-R7; dilution 1/100; Thermo Scientific, CA, USA). Recognition was accomplished by secondary antibodies and labeled horseradish peroxidase followed by colorimetric detection by 3, 30-diaminobenzidine (DAB). Hematoxylin was used as a counterstain. Negative control slides were put in phosphate-buffered saline as a replacement for the primary antibody. Under light microscope, the brown color indicated the antigen
site (Ramos-Vara et al. 2008).

Transmission electron microscope (TEM) study

Fixation of the specimens was done by phosphate-buffered glutaraldehyde (pH 7.4), and post fixation by 1% osmium tetroxide at 4 ◦C. The specimens then dehydrated and embedded in epoxy resin.
Cutting by Leica ultra-cut (UCT) and staining by uranyl acetate and lead citrate were performed (Ayache et al. 2010). Ultrathin sections (50 nm thick) were checked and photographed using TEM (JEOL JEM 1010; Jeol Ltd., Tokyo, Japan) in the Regional Center of Mycology and Biotechnology, Al-Azhar University, Egypt.

Morphometric Study

The data were investigated by Leica QWin 500 software using digital camera linked to an optical microscope (Olympus, Tokyo, Japan). Positive brown cells were counted in anti-CbD28k, anti-JNK and

anti-NFκB immune-stained sections. In 7286, 78 μm^2 measuring frames at a magnification of 400×, ten non-overlapping fields from each rat were randomly selected and investigated by analyst who was unaware of the experiment.

The linear density of Purkinje cells was also measured in H&E stained sections. For each rat, Purkinje cells (recognized by nerve cell body) were counted in each of 10 intact cerebellar lobules of sagittal sections at 200× magnification, and then the mean value for each section was estimated. The density was calculated as the mean value of cell count per millimeter length of cerebellar tissue (McGoey et al. 2003).

Statistical Analysis

Statistical Package for Social Sciences (SPSS) version 22.0 (IBM Corp., Armonk, NY, USA) was used to analyze the data. Values were expressed as mean ± standard deviation (X±SD). ANOVA test followed by Tukey's post-hoc test was used. The probability values (*p*) less than 0.05 were regarded as significant and highly significant with *p* values less than 0.001.

Results

Characterization of Ag-NPs

They appeared spherical with diameters<100nm (average 83±37nm) **(Fig. 1A)**.

Biochemical and Molecular results

Measurements of serum proinflammatory cytokines

Measurements of IL-1β and TNF-α demonstrated significant increases in the low-dose group ($p<0.05$) and highly significant increases in the high-dose group ($p<0.001$) when compared to the control group. There was a non-statistically significant rise in IL-6 in the low-dose group ($p>0.05$), while there was a highly significant increase in the high-dose group ($p<0.001$) compared to the control (Table 2).

Table 2 Biochemical parameters

	Group I	Group II	Group III	Group IV
IL-1β (pg/ml)	37.2±7.6	35.3±6.6	52.3±13.0*	123.6±12.1**
IL-6 (pg/ml)	18.4±5.5	19.0±4.7	38.7±4.1	138.2±5.7**
TNF-α (pg/ml)	10.3±1.9	11.0±3.4	18.2±4.5*	27.2±10.1**

TNF-α, tumor necrosis factor-alpha; IL-1β, interleukin-1 beta; IL-6, interleukin-6. Values are expressed as mean ± standard deviation (X ± SD); *: significant difference ($P<0.05$); **: highly

significant difference *(P*<0.001); n = 10 animals.

Real-time PCR analysis of apoptotic and oxidative stress genes

Statistical analysis of the mean Ddit4 and Txnip mRNA levels showed significant increases in the low-dose group (p<0.05) and highly significant increases in the high-dose group (p<0.001) compared to normal controls. The increase was non-statistically significant regarding the mean FMO2 mRNA level in the low-dose group (p>0.05) but highly significant in the high-dose group (p<0.001) in comparison with normal controls (Fig. 1 B, C& D).

Histopathological results

The control groups I and II exhibited almost similar results. Accordingly, only group I results were presented in figures.

SEM and EDX analysis results

SEM image and EDX spectrum analyses indicated the presence of considerable amounts of Ag-NPs in the cerebellar cortex, which increased in a dose-dependent manner in the exposure groups (Fig. 2).

H&E results

Light microscope examination of H&E-stained sections of the control group showed that the outer molecular layer was formed of fibers mainly with few scattered cells. The middle layer contained one row of flask-shaped Purkinje cells and Bergmann astrocytes. Purkinje cells had rounded vesicular nuclei with prominent nucleoli. Granular layer had small closely packed granule cells together with non-cellular cerebellar islands (Fig. 3A). In group III, the molecular layer showed some spaces. Some Purkinje cells appeared normal while others appeared atrophied, shrunken with ill-defined nuclei and surrounded by vacuolar spaces. Some cells of the granular layer appeared with darkly stained nuclei (Fig. 3B). In group IV, the molecular layer contained many vacuolar spaces and pyknotic nuclei. Purkinje cells appeared distorted, shrunken with pyknotic ill-defined nuclei and acidophilic cytoplasm, and surrounded by vacuolar spaces. Areas of focal loss in neurons were also seen. Bergman astrocytes appeared swollen with dark nuclei and wide perinuclear spaces. Some granular layer cells had darkly stained nuclei with spaces in between. Cerebellar islands showed vacuolations (Fig. 3C).

Immunohistochemical results

Immunohistochemically stained sections for CB of group I showed positive cytoplasmic immune reaction in most of Purkinje cells (Fig.4A), few immune reactive cells were detected in group III (Fig. 4B), while the reactions were nearly absent in group IV (Fig. 4C).

Group I sections stained for JNK revealed scanty positive immune reactions (Fig. 4D). Some positive immunoreactions were detected in the granular layer of group III sections (Fig. 4E). In group IV, many immune reactions were seen all over the three layers of the cerebellar cortex (Fig. 4F).

NF-κB-stained sections showed very few immune reactions in group I (Fig. 4G). In group III, brown immune reactions in some cells were seen (Fig. 4H), and several positive cells appeared in group IV (Fig. 4I).

Ultrastructure results

TEM examination of the cerebellar cortex of group I revealed that the molecular layer was formed of compact full neuropil (dendrites, unmyelinated axons, processes of neuroglia) and neuroglia in-between (Fig. 5A). Purkinje cells appeared with regular contour, euchromatic indented nuclei, prominent nucleoli, and clear cytoplasm with short profiles of rough endoplasmic reticulum cisternae, mitochondria and free ribosomes. They were surrounded by tight neuropil and blood capillaries (Fig. 5D). Astrocytes had euchromatic nuclei and surrounded by a shell of cytoplasm filled with organelles. Adjacent blood capillaries were seen separated by narrow perivascular spaces. They had regular lumen, smooth endothelial lining and mitochondria with intact cristae in the cytoplasm of endothelium and pericytes (Fig. 6 A&B). The granular layer had well-defined ring-shaped cerebellar islands that contained myelinated fibers with spherical mitochondria, and mossy rosettes with many mitochondria. The granule cells had rounded euchromatic nuclei with peripheral clumps of heterochromatin surrounded by a shell of cytoplasm containing mitochondria, strands of rough endoplasmic reticulum and free ribosomes. In the vicinity, neuroglia had darker nuclei with marginal heterochromatin and electron dense cytoplasm (Fig. 6 E&F).
Group III ultrathin sections showed the molecular layer with some areas of vacuolated neuropil, vacuoles within some axons and neuroglia (Fig. 5B). Purkinje cells showed darker nuclei, prominent nucleoli and dimples in the nuclear envelope, some dilated cisternae of rough endoplasmic reticulum and some vacuoles in the cytoplasm. The cells were surrounded by loose vacuolar spaces (Fig. 5E). Perivascular astrocytes showed increased translucence of their cytoplasm. Mitochondria with ruptured cristae were found in the cytoplasm of astrocytes, capillary endothelium and pericytes (Fig. 6C). In the granular layer, some nerve fibers showed disruption or splitting of myelin sheaths. Granule neurons appeared with increased condensation of nuclear chromatin, some vacuoles in the perikaryon and some areas of vacuolated neuropil between the cells. Electron dense silver nanoparticles could be detected within the neuropil (Fig. 6G&H).

In ultrathin sections of group IV, most of the neuropil of the molecular layer appeared vacuolated and vacant; the neuroglia had many large vacuolar spaces (Fig. 5C). Purkinje neurons showed irregular cell membrane and a shadow of muddy ill-defined nucleus. The cytoplasm contained dilated cisternae of rough endoplasmic reticulum and vacuoles. The cell was surrounded by vacuolated neuropil. Fragments of Purkinje cells perikaryon appeared electron dense with dilated rough endoplasmic reticulum cisternae (Fig. 5F&G). Swollen astrocytes showed clumps of heterochromatin within and around the edge of the

nuclei, increased matrix translucence and loss of cytoplasmic organelles. Blood capillaries were surrounded by a large perivascular space. The lining endothelium showed mitochondria with ruptured crista and separation of the basement membrane (Fig. 5G&6D). Granular layer showed irregularly arranged neurons with heterochromatic nuclei and intracellular vacuolar spaces. Cerebellar islands were distorted. Many fibers showed splitting of myelin sheath and some appeared ballooned or empty with wide spaces in-between. Adjacent neuroglia appeared with heterochromatic nuclei and surrounded by vacuolated neuropil. Electron dense silver nanoparticles could be detected within the neuropil (Fig.6I&J).

Morphometric results

Statistically analyzed results of numbers of CB, JNK and NF-κB in immune-stained sections and Purkinje cell linear density in H&E sections were represented in (Table 3).

Table 3 Number of anti-JNK, anti-NF-κB immune-stained cells, anti- CB and Purkinje cell linear density

	Group I	Group II	Group III	Group IV
Anti- CB	10.2±2.6	10.5±2.8	5.6±3.0*	1.1±1.0**
Anti- JNK	0.9±0.6	1.3±0.7	28.2±7.7**	103.1±14.7**
Anti- NF-κB	1.6±1.1	1.8±0.9	17.6±6.0**	36.9±8.3**
Purkinje cell linear density	19.5±3.6	20.2±3.6	13.9±2.6*	8.0±2.2**

CB, Calbindin D28k; JNK, c-Jun N-terminal kinase; NF-κB, nuclear factor kappa beta. Values are expressed as mean ± standard deviation (X ± SD); *: significant difference ($P<0.05$); **: highly significant difference ($P<0.001$); n = 10 animals.

Discussion

The excessive applications of nano-silver cause wide environmental contamination and raise the hazards of human exposure (Liao et al. 2019). The brain is a highly vulnerable organ to silver toxicity due to the prolonged exposure caused by the long biological half-life of silver in the CNS when compared with other organs (Yang et al. 2010). It was found that silver was removed from most organs, except brain and testis after 8 weeks in rats exposed to oral Ag-NPs for 28 days (van der Zande et al. 2012). The existence of blood brain barrier (BBB) could decrease the rate of Ag-NPs clearance from the brain that leads to long standing adverse effects in brain tissue (Lee et al. 2013).

Ag-NPs cause tissue damage due to direct deposition in the
tissues owing to their small size. Also, they release large amount of free toxic silver ions (Ag^+) (Amin et al. 2015). Neurons are more sensitive to nano-silver because of their high metabolic requirements (Entezari et al. 2013). On comparing particle sizes; the smaller the size, the more severe adverse effects occur (Gromadzka-Ostrowskaa et al. 2012).

In the current study, Ag-NPs exposure severely disrupted the architecture of the cerebellar cortex. The disruption was more apparent in the high-dose group compared with the low-dose group. Purkinje and granule neurons displayed marked alterations. The cytoplasm of the degenerated Purkinje neurons appeared deeply acidophilic which was known as ‘eosinophilic neuron degeneration’ or ‘red dead neurons’. Vacuolated neuropils might result from degeneration and shrinkage of Purkinje cells with retraction of their processes leaving empty spaces. Others explained vacuolations by swelling of processes of degenerated neurons or activated glial cells (Garman et al. 2011). Areas of focal loss in neurons were also seen. This was confirmed by the morphometric measurement of the linear density of Purkinje cells that revealed a significant and a highly significant reduction in the low-dose and high-dose group respectively compared with the control. These results were in harmony with Xu et al. (2013) who found in their in vitro study that 20 nm Ag-NPs hinder the sprouting of neuronal outlets or elongation of axons, and produced neurotic processes degeneration. Moreover, Ag-NPs decreased cytoskeletal integrity, synaptic proteins, mitochondrial function and so cell viability.

TEM pictures of treated groups of this study revealed cells having degenerated mitochondria with ruptured cristae. Similar results were seen with Zhang et al. (2015). It is well known that silver nanoparticles cause decreased ATP levels and so discomposure of cellular respiration leading to mitochondrial damage and cell death (Costa et al. 2010). Another ultrastructural finding, in the current work, was the dilated RER in Purkinje cells. This was in line with the findings of Zhang et al. (2012) who stated that treatment of liver cells by nano-silver ($\leq$100nm) induced endoplasmic reticulum stress and increased the levels of chaperone proteins (ER membrane proteins that act as sensors for ER stress). The over-expression of these chaperones leads to inhibition of protein translation. Simard et al. (2016) added that this ER stress response pathway may extend to cell death. We also noticed splitting of the myelin sheaths of some nerve fibers in Ag-NPs-intoxicated groups. Similarly, Dąbrowska-Bouta et al. 2019 reported myelin disintegration after 2-week-exposure to oral nano-silver (0.2 mg/kg) in rats. The previous researchers concluded that oxidative stress affects the proper structure of myelin sheaths by disrupting the lipid and protein constituents of myelin membranes.

In the present study, TEM findings revealed that Ag-NPs induced BBB destruction as evident from, (i) astrocytes appeared swollen with loss of cytoplasmic organelles; (ii) the capillaries were surrounded by wide perivascular spaces; (iii) the lining endothelium had degenerated mitochondria. Other studies also revealed similar results in brain owed to a low dose of Ag-NP exposure by oral route (Skalska et al. 2015). Another in vitro study showed that citrate coated Ag-NPs led to brain endothelial cell membrane damage and disrupt colony formation (Grosse et al. 2013). Astrocyte revealed the appearance of nano-silver-like particles (Xu et al. 2015a). Ag^+ ions trigger cell necrosis in astrocytes through disrupting the integrity of

cell membrane and binding with cellular thiol groups. On the other hand, Ag-NPs stimulates apoptosis by mediating production coupled with JNK activation (Sun et al. 2016). Ag-NPS intoxication reduces the biosynthetic activities in astrocytes e.g. nerve growth factor (Nr4a1) secretion that could affect neuronal survival and protection (Xu et al. 2015b). Rafati et al (2015) added that degeneration of glial cells causes also degeneration of cerebellar Purkinje cells.

Notably, we observed that Ag-NPs intake elicited different nuclear responses in light and electron microscope slides; some nuclei seemed small and pyknotic, others appeared irregular with clumping of chromatin. These findings were in line with Hackenberg et al. (2011) who reported that deposition of nano-silver in the nuclei of mesenchymal stem cells triggered DNA damage which appeared as chromatid deletions and chromatid exchanges. Cell cycle arrest also happened in the G2/M phase in cells treated with high dose of nano-silver (7.5 nm). In the present work, gene expression analysis of Ddit4 revealed that Ag-NPs exposure significantly increase Ddit4 mRNA in a dose depending manner. Ddit4 is believed to enhance apoptosis and decrease cell proliferation (Lisse et al. 2011). Ag-NPs were accompanied by cellular death more than 30% (Kang et al. 2012).

In the same context, we detected a significant increase in immune histochemical expressions of the apoptotic marker JNK in Ag-NPs-exposure groups. These results conform to the results of Rinna et al. (2015). The key cytotoxic effect of Ag-NPs is apoptosis-mediated cell death (Gusseme et al. 2011). Hsin et al. (2008) demonstrated that nano-silver encourages ROS generation leading to the activation of JNK and p53, and cytochrome c release which progresses to apoptosis. The excess production of ROS intern increases the pro-apoptotic kinase p38 and decreases PARP (poly ADP ribose polymerase) resulting in significant surge of caspase-3 and total p53 expressions (Li et al. 2016). So, nano-silver triggers both the mitochondrial and the extrinsic apoptotic pathways (Hadrup et al. 2012). Yin et al. (2015) reported that granule cells are the most vulnerable cells to NPs. JNK also stimulates the phosphorylation of the BH3-only protein BAD (proteins promote cell death) in cerebellar granule neurons promoting apoptosis by another mechanism (Donovan et al. 2002). Yin et al. (2013) accused the oxidative cell damage by the aroused ROS to be the cause of apoptosis.

Ag-NPs act as catalyst that directly produces ROS especially in the presence of oxygen. In addition, Silver itself has strong affinity for sulfur present in cellular protein (Xu et al. 2012). The present study proposed oxidative stress as an adverse effect of Ag-NPs exposure. We recorded enhancement of Txnip gene expression in Ag-NPs treated groups. Txnip, a member of α-arrestin family, is implicated in redox sensing. Up-regulation of Txnip increases ROS and compromises the antioxidant capacity of the brain (Junn et al. 2000). We also detected upregulation of FMO2 gene expression (the gene responsible for oxidation of reduced glutathione GSH) following Ag-NPs exposure. Rahman et al. (2009) added that these changes disrupt oxidized glutathione GSSG/GSH balance.

Regarding the inflammatory responses elicited by Ag-NPs exposure, we revealed a significant enhancement of NF-κB immune expressions in nano-silver treated groups. We also found statistically significant increases of the serum inflammatory cytokines; IL-1β, IL-6 and TNF-α following Ag-NPs

administration in a dose-dependent manner. This could be explained by the excess release of ROS. Perrone et al., (2009) declared that Txnip up-regulation stimulates the activation of NF-κB and the release the pro-inflammatory mediators such as TNF-α and IL-1β. In line with our results, in vivo oral nano-silver (22, 42, 71 nm) given 1 mg/kg for 14 days elevated the serum levels of TGF-β, IL-1, IL-4, IL-6, IL-12 and increased delivery of B cells and natural killer cells (Park et al. 2010). Prasad et al. (2013) showed that nano-silver (10 and 75 nm) motivated inflammation in vitro by stimulating NF-κB and AP1 pathways. Interestingly, JNK is activated by inflammatory mediators such as IL-6 and TNF-α; activated JNK phosphorylates c-Jun (a component of AP-1 complex); AP-1 complex controls the transcription of inflammation-related genes; all these events aggravate inflammation (Assi et al. 2006).

Nano-silver increases the intracellular calcium levels in neuron-enriched culture (Haase et al. 2012). That calcium homeostasis deterioration is one of the key mechanisms of Ag-NPs neurotoxicity (Ziemińska et al. 2014). When N-methyl-d-aspartate receptors are over-activated by nano-silver; calcium overflows into cells, excessively taken by mitochondria causing mitochondrial degeneration and dysfunction leading to generation of ROS and apoptosis (Saliñska et al. 2005). CB is a calcium-binding protein that maintains calcium homeostasis. CB plays a pivotal role in preventing neuronal death by blocking several pro-apoptotic pathways (Kook et al. 2014). CB protects against oxidative stress and toxic agents (Yuan et al. 2013). CB level significantly diminishes during degenerative neuronal diseases (Servais et al. 2005). In nano-silver exposed groups, we reported a significant decline in immune expressions of CB in Purkinje cells. Depletion of CB reduces the buffering capacity of neurons and causing increase of intracellular and intranuclear calcium (Katsetos et al. 2001).

Conclusion

Ag-NPs exposure provoked biochemical, cellular and molecular changes of rat cerebellar cortex in a dose-dependent manner. The key mechanisms included activation of apoptosis cascades coupled with stimulation of oxidative stress and inflammation pathways. This was evident by the upregulation of Ddit4 gene expressions and JNK protein immune expressions. Alterations of redox homeostasis were verified by enhancement of Txnip and FMO2 gene expressions, favoring the activation of inflammatory responses and increases in NFκB immune expressions and serum inflammatory mediator levels (IL-1B, IL6 and TNF-α). Another considerable cytotoxic effect of nano-silver was the reduction of CB immune expressions, the crucial regulator of intracellular calcium level.

Abbreviations

Ag-NPs: Silver nanoparticles

BBB: Blood brain barrier

CB: Calbindin D28k

Ddit4: DNA damage inducible transcript 4

EDX detector: Energy dispersive X-ray detector

ER: Endoplasmic reticulum

FMO2: Flavin containing monooxygenase 2

GSH: Reduced glutathione

GSSG: Oxidized glutathione

H&E: Hematoxylin and Eosin

IACUC: Institutional Animal Care and Use Committee

IL-1β: Interleukin-1 beta

IL-6: Interleukin-6

JNK: c-Jun N-terminal kinase

NF-κB: Nuclear factor kappa beta

PCR: Transcription polymerase chain reaction

PVP: Poly vinyl pyrrolidone

ROS: Reactive oxygen species

SEM: Scanning electron microscopy

SPSS: Statistical Package for Social Sciences

TEM: Transmission electron microscope

TNF-α: Tumor necrosis factor-alpha

Txnip: Thioredoxin-interacting protein

Declarations

Availability of data and materials

The data supporting the conclusions of this article will be made available by the authors, without undue reservation, to any qualified researcher.

Authors' Contributions

EMM assisted in acquisition of data and drafting of the manuscript; AAK shared in data interpretation and statistical analysis; RSA guided biochemical analysis, SAA handled image acquisition and analysis. All authors assisted in designing the research and approved the final version to be submitted.

Acknowledgments

Conflicts of interest

The authors declare that they have no conflict of interest.

Funding

This study was not funded by any source.

Authors' Contributions

EMM assisted in acquisition of data and drafting of the manuscript; AAK shared in data interpretation and statistical analysis; RSA guided biochemical analysis, SAA handled image acquisition and analysis. All authors assisted in designing the research and approved the final version to be submitted.

Ethics declarations

Ethics

All procedures were done according to institutional guidelines for the use of experimental animals and approved by Institutional Animal Care and Use Committee IACUC (protocol approval number: 6937), Zagazig University, Egypt.

Consent for publication

This manuscript is solely submitted to *Molecular Medicine* and is not under consideration at any other journal nor has any part been previously published.

Competing interests

The authors report no proprietary or commercial interest in any product mentioned or concept discussed in this article.

References

Amin YM, Hawas AM, El-Batal AI, Elsayed SH. Evaluation of acute and subchronic toxicity of silver nanoparticles in normal and irradiated animals. Br J Pharmacol and Toxicol. 2015;6(2):22-38.

Assi K, Pillai R, Gómez-Muñoz A, Owen D, Salh B. The specific JNK inhibitor SP600125 targets tumour necrosis factor-α production and epithelial cell apoptosis in acute murine colitis. Immunology

2006;118(1):112-21.

Ayache J, Beaunier L, Boumendil J, Ehret G, Laub D. Sample Preparation Handbook for Transmission Electron Microscopy Techniques. New York: Springer Science and Businesss Media; 2010.

Bancroft JD, Gamble M. Theory and Practice of Histological Techniques. 6th ed. London: Churchill Livingstone;2008.

Barski JJ, Hartmann J, Rose CR, Hoebeek F, Mörl K, Noll-Hussong M, et al. Calbindin in cerebellar Purkinje cells is a critical determinant of the precision of motor coordination. J Neurosci. 2003;23(8):3469-77.

Costa CS, Ronconi JV, Daufenbach JF, Gonçalves CL, Rezin GT, Streck EL, et al. In vitro effects of silver nanoparticles on the mitochondrial respiratory chain. Mol Cell Biochem. 2010;342(1-2):51-6.

Dąbrowska-Bouta B, Sulkowski G, Strużyński W, Strużyńska L. Prolonged exposure to silver nanoparticles results in oxidative stress in cerebral myelin. Neurotox Res. 2019;35(3):495-504.

Dhanasekaran DN, Reddy EP. JNK signaling in apoptosis. Oncogene. 2008;27(48):6245-51.

Donovan N, Becker EB, Konishi Y, Bonni A. JNK phosphorylation and activation of BAD couples the stress-activated signaling pathway to the cell death machinery. J Biol Chem. 2002;277(43):40944-9.

Entezari M, Safari M, Hekmati M, Hekmat S, Azin A.Modification of carboxylated multiwall nanotubes with benzotriazole derivatives and study of their anticancer activities. Med Chem Res. 2013;23(1):487-495.

Garman RH. Histology of the central nervous system. J Toxicol Pathol. 2011;39(1):22-35.

Gromadzka-Ostrowska J, Dziendzikowska K, Lankoff A, Dobrzyńska M, Instanes C, Brunborg G, et al. Silver nanoparticles effects on epididymal sperm in rats. Toxicol Lett 012;214(3):251-8.

Grosse S, Evje L, Syversen T. Silver nanoparticle-induced cytotoxicity in rat brain endothelial cell culture. Toxicol In Vitro. 2013; 27(1): 305-313.

Gusseme DB, Hennebel T, Christiaens E, Saveyn H, Verbeken K, Fitts JP, et al. Virus disinfection in water by biogenic silver immobilized in polyvinylidene fluoride membranes. Water Res 2011;45(4):1856–64.

Haase A, Rott S, Mantion A, Graf P, Plendl J, Thünemann AF, et al. Effects of silver nanoparticles on primary mixed neural cell cultures: uptake, oxidative stress and acute calcium responses. Toxicol Sci 2012;126(2):457-68.

Haase A, Tentschert J, Jungnickel H, Graf P, Mantion A, Draude F, et al. Toxicity of silver nanoparticles in human macrophages: uptake, intracellular distribution and cellular responses. J Phys Conf Ser. 2011;304(1): 012030.

Hackenberg S, Scherzed A, Kessler M, Hummel S, Technau A, Froelich K, et al. Silver nanoparticles: evaluation of DNA damage, toxicity and functional impairment in human mesenchymal stem cells. Toxicol Lett. 2011;201(1):27-33.

Hadrup N, Loeschner K, Mortensen A, Sharma AK, Qvortrup K, Larsen EH, et al. The similar neurotoxic effects of nanoparticulate and ionic silver in vivo and in vitro. Neurotoxicology. 2012;33(3):416-23.

Hsin YH, Chen CF, Huang S, Shih TS, Lai PS, Chueh PJ. The apoptotic effect of nanosilver is mediated by a ROS-and JNK-dependent mechanism involving the mitochondrial pathway in NIH3T3 cells. Toxicol Lett. 2008;179(3):130-9.

Junn E, Han SH, Im JY, Yang Y, Cho EW, Um HD, Lee KW, Han PL, Rhee SG, Choi I. Vitamin D3 up-regulated protein 1 mediates oxidative stress via suppressing the thioredoxin function. J Immunol. 2000;164(12):6287-95.

Kang SJ, Lee YJ, Lee EK, Kwak MK. Silver nanoparticles-mediated G2/M cycle arrest of renal epithelial cells is associated with NRF2-GSH signaling. Toxicol Lett 2012;211(3):334-41.

Katsetos CD, Spandou E, Legido A, Taylor ML, Zanelli SA, de Chadarevian JP, et al. Acute hypoxia-induced alterations of calbindin-D28k immunoreactivity in cerebellar Purkinje cells of the guinea pig fetus at term. J Neuropathol Exp Neurol. 2001;60(5):470-82.

Kim YS, Kim JS, Cho HS, Rha DS, Kim JM, Park JD, et al. Twenty-eight-day oral toxicity, genotoxicity, and gender-related tissue distribution of silver nanoparticles in Sprague-Dawley rats. Inhal Toxicol. 2008;20(6):575-83.

Kook SY, Jeong H, Kang MJ, Park R, Shin HJ, Han SH, et al. Crucial role of calbindin-D 28k in the pathogenesis of Alzheimer's disease mouse model. Cell Death Differ. 2014;21(10):1575-87.

Lee JH, Kim YS, Song KS, Ryu HR, Sung JH, Park JD, et al. Biopersistence of silver nanoparticles in tissues from Sprague–Dawley rats. Part Fibre Toxicol 2013;10(1):36.

Li L, Xu Z, Wimmer A, Tian Q, Wang X. New insights into the stability of silver sulfide nanoparticles in surface water: dissolution through hypochlorite oxidation. Environ Sci Technol. 2017;51(14):7920-7.

Li Y, Guo M, Lin Z, Zhao M, Xiao M, Wang C, et al. Polyethyleniminefunctionalized silver nanoparticle-based co-delivery of paclitaxel to induce HepG2 cell apoptosis. Int J Nanomed 2016; 11:6693–702.

Liao C, Li Y, Tjong SC. Bactericidal and cytotoxic properties of silver nanoparticles. Int J Mol Sci. 2019;20(2):449.

Lisse TS, Liu T, Irmler M, Beckers J, Chen H, Adams JS, et al. Gene targeting by the vitamin D response element binding protein reveals a role for vitamin D in osteoblast mTOR signaling. The FASEB J. 2011;25(3):937-47.

Liu W, Wu Y, Wang C, Li HC, Wang T, Liao CY, et al. Impact of silver nanoparticles on human cells: effect of particle size. Nanotoxicology. 2010; 4(3):319–30.

Livak KJ, Schmittgen TD. Analysis of relative gene expression data using real-time quantitative PCR and the 2− ΔΔCT method. Methods. 2001;25(4):402-8.

McGoey TN, Reynolds JN, Brien JF. Chronic prenatal ethanol exposure-induced decrease of guinea pig hippocampal CA1 pyramidal cell and cerebellar Purkinje cell density. Can J Physiol Pharmacol 2003;81(5):476-84.

Murugan K, Choonara YE, Kumar P, Bijukumar D, du Toit LC, Pillay V. Parameters and characteristics governing cellular internalization and trans-barrier trafficking of nanostructures. Int J Nanomed. 2015; 10:2191.

Ndukwu MC, Ikechukwu-Edeh CE, Nwakuba NR, Okosa I, Horsefall IT, Orji FN. Nanomaterials application in greenhouse structures, crop processing machinery, packaging materials and agro-biomass conversion. Mater Sci Technol. 2020; 3:690-699.

Oberdörster G, Elder A, Rinderknecht A. Nanoparticles and the brain: cause for concern? J Nanosci Nanotechnol. 2009;9(8):4996-5007.

Park EJ, Bae E, Yi J, Kim Y, Choi K, Lee SH, et al. Repeated-dose toxicity and inflammatory responses in mice by oral administration of silver nanoparticles. Environ Toxicol Pharmacol 2010;30(2):162-8.

Patra JK, Baek KH. Antibacterial activity and synergistic antibacterial potential of biosynthesized silver nanoparticles against foodborne pathogenic bacteria along with its anticandidal and antioxidant effects. Front Microbiol. 2017; 8:167.

Perrone L, Devi TS, Hosoya KI, Terasaki T, Singh LP. Thioredoxin interacting protein (TXNIP) induces inflammation through chromatin modification in retinal capillary endothelial cells under diabetic conditions. J Cell Physiol. 2009;221(1):262-72.

Prasad RY, McGee JK, Killius MG, Suarez DA, Blackman CF, DeMarini DM et al. Investigating oxidative stress and inflammatory responses elicited by silver nanoparticles using high-throughput reporter genes in HepG2 cells: effect of size, surface coating, and intracellular uptake. Toxicol Vitr 2013; 27(6).

Rafati A, Erfanizadeh M, Noorafshan A, KarbalayDoust S. Effect of benzene on the cerebellar structure and behavioral characteristics in rats.
Asian Pac J Tropi Biomed 2015; 5(7):568-573.

Rahman MF, Wang J, Patterson TA, Saini UT, Robinson BL, Newport GD, et al. Expression of genes related to oxidative stress in the mouse brain after exposure to silver-25 nanoparticles. Toxicol Lett. 2009; 187(1): 15-21.

Ramos-Vara, JA, Kiupel M, Baszler T, Bliven L, Brodersen B, Chelack B et al. Suggested guidelines for immunohistochemical techniques in veterinary diagnostic laboratories. J Vet Diagn Investig.2008; 20: 393–413.

Rinna A, Magdolenova Z, Hudecova A, Kruszewski M, Refsnes M, Dusinska M. Effect of silver nanoparticles on mitogen-activated protein kinases activation: role of reactive oxygen species and implication in DNA damage. Mutagenesis. 2015;30(1):59-66.

Saliñska E, Danysz W, Łazarewicz JW. The role of excitotoxicity in neurodegeneration. Folia Neuropathol. 2005;43(4).

Servais L, Bearzatto B, Schwaller B, Dumont M, De Saedeleer C, Dan B, et al. Mono-and dual-frequency fast cerebellar oscillation in mice lacking parvalbumin and/or calbindin D-28k. Eur J Neurosci. 2005;22(4):861-70.

Simard JC, Durocher I, Girard D. Silver nanoparticles induce irremediable endoplasmic reticulum stress leading to unfolded protein response dependent apoptosis in breast cancer cells. Apoptosis. 2016;21(11):1279-90.

Skalska J, Frontczak-Baniewicz M, Struzynska L. Synaptic degeneration in rat brain after prolonged oral exposure to silver nanoparticles. Neuro Toxicol 2015;46:145–54.

Stoehr LC, Gonzalez E, Stampfl A, Casals E, Duschl A, Puntes V, et al. Shape matters: effects of silver nanospheres and wires on human alveolar epithelial cells. Part Fibre Toxicol. 2011;8(1):425–30.

Strick PL, Dum RP, Fiez JA. Cerebellum and nonmotor function. Annu Rev Neurosci. 2009; 32:413-34.

Sun C, Yin N, Wen R, Liu W, Jia Y, Hu L, et al. Silver nanoparticles induced neurotoxicity through oxidative stress in rat cerebral astrocytes is distinct from the effects of silver ions. Neurotoxicology 2016; 52:210-21.

Tang J, Xiong L, Zhou G, Wang S, Wang J, Liu L, et al. Silver nanoparticles crossing through and distribution in the blood-brain barrier in vitro. J Nanosci Nanotechnol. 2010;10(10):6313-7.

Trickler WJ, Lantz SM, Murdock RC, Schrand AM, Robinson BL, Newport GD, et al. Silver nanoparticle induced blood-brain barrier inflammation and increased permeability in primary rat brain microvessel endothelial cells. Toxicol Sci. 2010; 118:160–70.

van der Zande M, Vandebriel RJ, Van Doren E, Kramer E, Herrera Rivera Z, Serrano-Rojero CS, et al. Distribution, elimination, and toxicity of silver nanoparticles and silver ions in rats after 28-day oral exposure. ACS nano. 2012;6(8):7427-42.

Verdes JM, Moraña JA, Battes D, Gutiérrez F, Guerrero F, Goicoa A, et al. Calbindin D28k expression and the absence of apoptosis in the cerebellum of Solanum bonariense L–intoxicated bovines. Vet path.

2010;47(3):569-72.

Wang L, Zhang T, Li P, Huang W, Tang J, Wang P, Liu J, Yuan Q, Bai R, Li B, Zhang K. Use of synchrotron radiation-analytical techniques to reveal chemical origin of silver-nanoparticle cytotoxicity. ACS nano. 2015;9(6):6532-47.

Wijnhoven SW, Peijnenburg WJ, Herberts CA, Hagens WI, Oomen AG, Heugens EH, et al. Nano-silver–a review of available data and knowledge gaps in human and environmental risk assessment. Nanotoxicology. 2009 ;3(2):109-38.

Xiang DX, Chen Q, Pang L, Zheng CL. Inhibitory effects of silver nanoparticles on H1N1 influenza A virus in vitro. J Virol Methods. 2011; 178:137–42.

Xu F, Piett C, Farkas S, Qazzaz M, Syed NI. Silver nanoparticles (AgNPs) cause degeneration of cytoskeleton and disrupt synaptic machinery of cultured cortical neurons. Mol Brain. 2013; 6(29): 1-15.

Xu L, Dan M, Shao A, Cheng X, Zhang C, Yokel RA, et al. Silver nanoparticles induce tight junction disruption and astrocyte neurotoxicity in a rat blood–brain barrier primary triple coculture model. Int J Nanomedicine. 2015b; 10:6105.

Xu L, Li X, Takemura T, Hanagata N, Wu G, Chou LL. Genotoxicity and molecular response of silver nanoparticle (NP)-based hydrogel. J Nanobiotechnology. 2012; 10(16): 1-11.

Xu L, Shao A, Zhao Y, Wang Z, Zhang C, Sun Y, et al. Neurotoxicity of silver nanoparticles in rat brain after intragastric exposure. J Nanosci Nanotechnol. 2015a;15(6):4215-23.

Yang Z, Liu ZW, Allaker RP, Reip P, Oxford J, Ahmad Z, et al. A review of nanoparticle functionality and toxicity on the central nervous system. J R Soc Interface. 2010;7(4): S411-22.

Yin N, Liu Q, Liu J, He B, Cui L, Li Z, et al. Silver nanoparticle exposure attenuates the viability of rat cerebellum granule cells through apoptosis coupled to oxidative stress. Small. 2013; 9(9-10): 1831-1841.

Yin N, Yao X, Zhou Q, Faiola F, Jiang G. Vitamin E attenuates silver nanoparticle-induced effects on body weight and neurotoxicity in rats. Biochem Biophys Res Commun 2015;458(2):405-10.

Yuan HH, Chen RJ, Zhu YH, Peng CL, Zhu XR. The neuroprotective effect of overexpression of calbindin-D 28k in an animal model of Parkinson’s disease. Mol Neurobiol. 2013;47(1):117-22.

Zhang R, Piao MJ, Kim KC, Kim AD, Choi JY, Choi J, et al. Endoplasmic reticulum stress signaling is involved in silver nanoparticles-induced apoptosis. Int J Biochem Cell Biol. 2012;44(1):224-32.

Zhang XF, Choi YJ, Han JW, Kim E, Park JH, Gurunathan S, et al. Differential nanoreprotoxicity of silver nanoparticles in male somatic cells and spermatogonial stem cells. Int J Nanomed 2015; 10:1335.

Ziemińska E, Stafiej A, Strużyńska L. The role of the glutamatergic NMDA receptor in nanosilver-evoked neurotoxicity in primary cultures of cerebellar granule cells. Toxicology. 2014; 315:38-48.

Figures

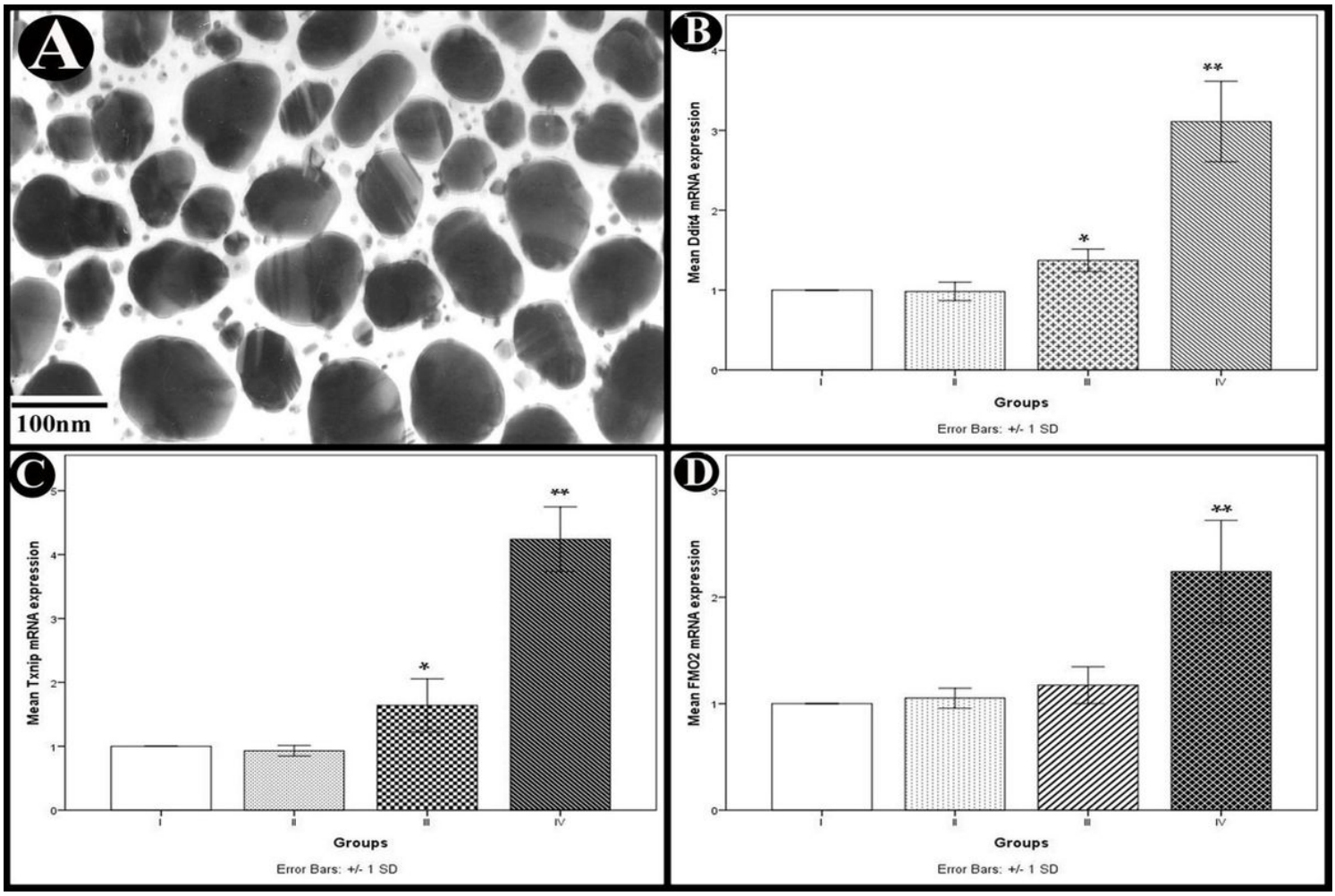

Figure 1

A, TEM image showing average diameters of Ag-NPs. B-D, Real-time PCR analysis of mRNA expressions of DNA damage inducible transcript 4 (Ddit4), thioredoxin-interacting protein (Txnip) and flavin containing monooxygenase 2 (FMO2) in the cerebellar cortex. Values are expressed as mean ± standard deviation (X ± SD); *: significant difference (P<0.05); **: highly significant difference (P<0.001); n = 10 animals.

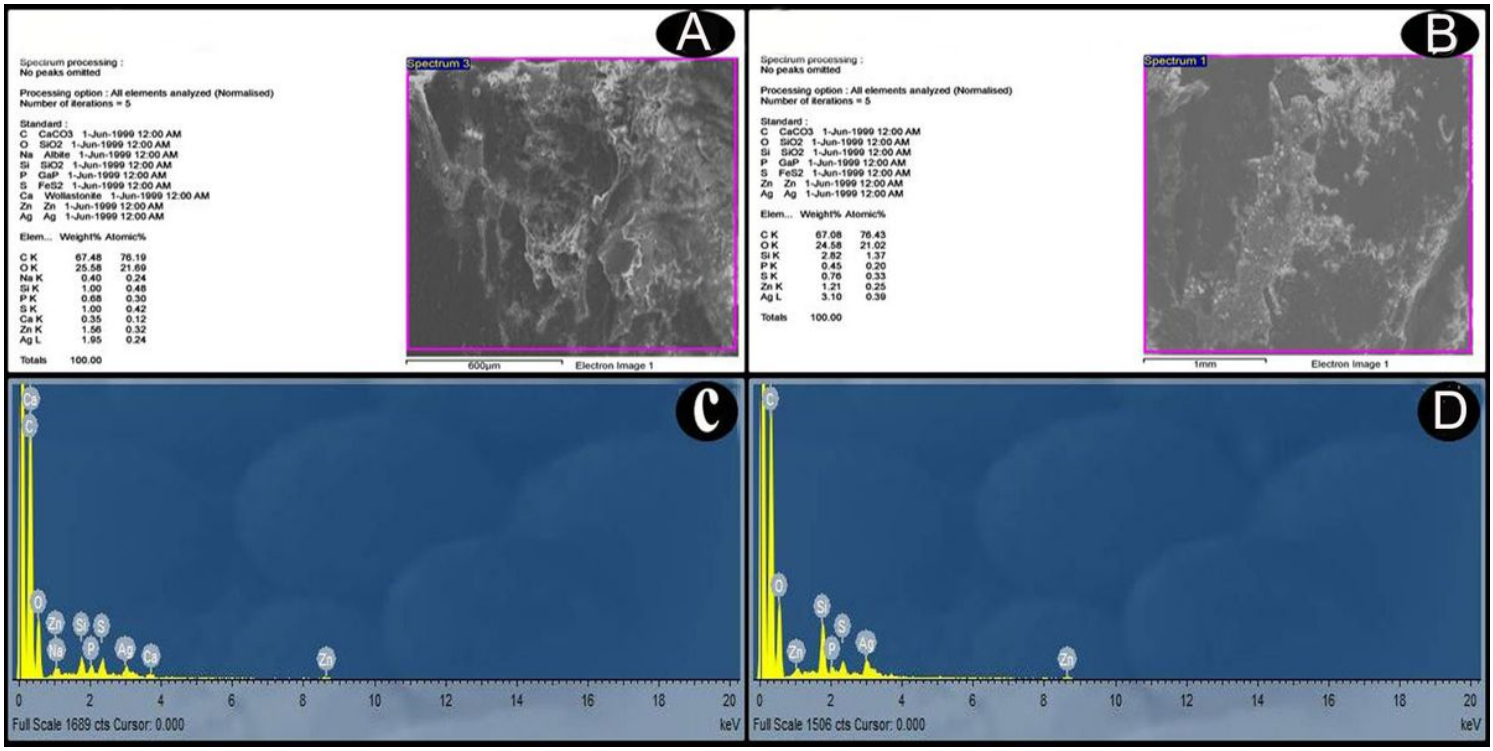

Figure 2

A & B, SEM images; backscattered electron images show contrast due to different element compositions for group III and IV respectively. C & D, Analyses of EDX for detection of these elements and their relative amounts (atomic % and weight %) by the production of an x-ray spectrum from the whole scan area of the SEM. The Y-axis represents the sums of x-rays and the X-axis depicts their energy level (KeV). The elements are identified by the place of the peaks, while the height of the peaks is used to measure the quantity of each element. C, Group III EDX spectrum shows a significant amount of Ag (one prominent peak at 3 KeV). D, Group IV EDX spectrum shows increased the amount of Ag compared with group III (one prominent peak at 3 KeV).

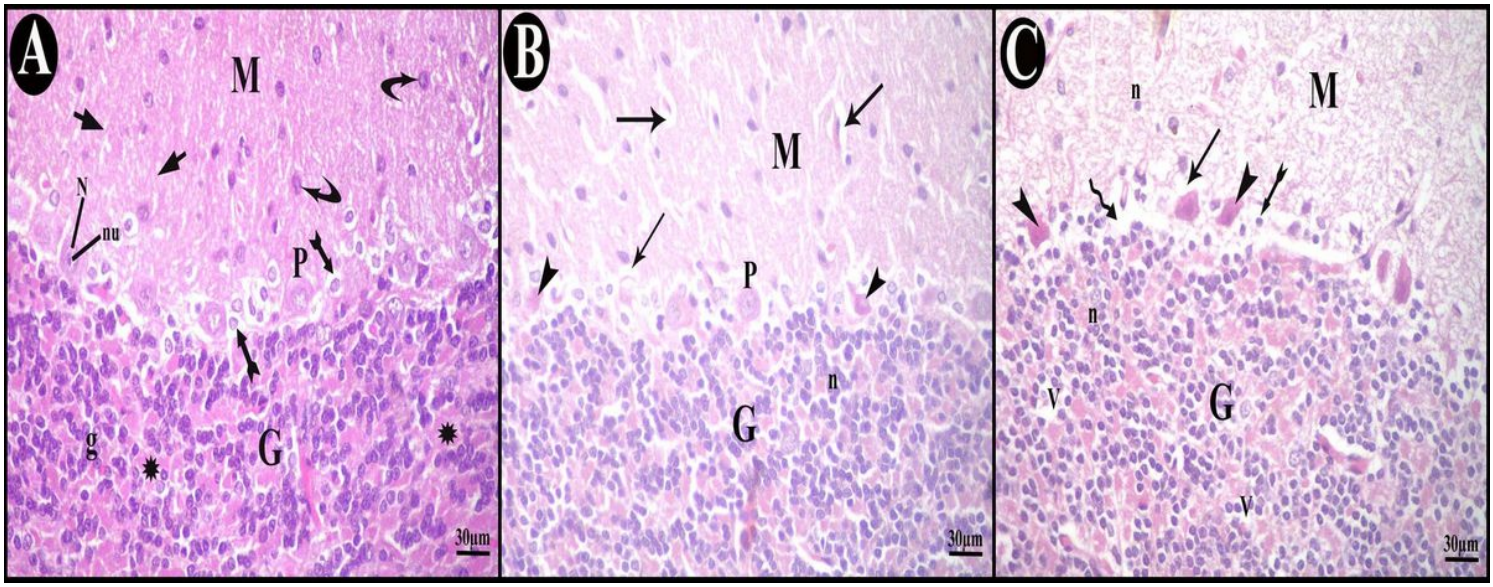

Figure 3

H&E-stained sections in adult albino rats' cerebellar cortex of the study groups. A, Control group. B, Group III. C, Group IV. Outer molecular layer (M), fibers (short arrow), scattered cells (curved arrow), normal Purkinje cells (P), Bergmann astrocytes (tailed arrow), nuclei of Purkinje cells (N), nucleoli of Purkinje cells (nu), granular layer (G), granule cells (g), non-cellular cerebellar islands (asterisk), vacuolar spaces (arrow), atrophied shrunken Purkinje cells (arrow head), cells having darkly stained nuclei (n), areas of focal neuron loss (zigzag arrow), vacuolations (V).

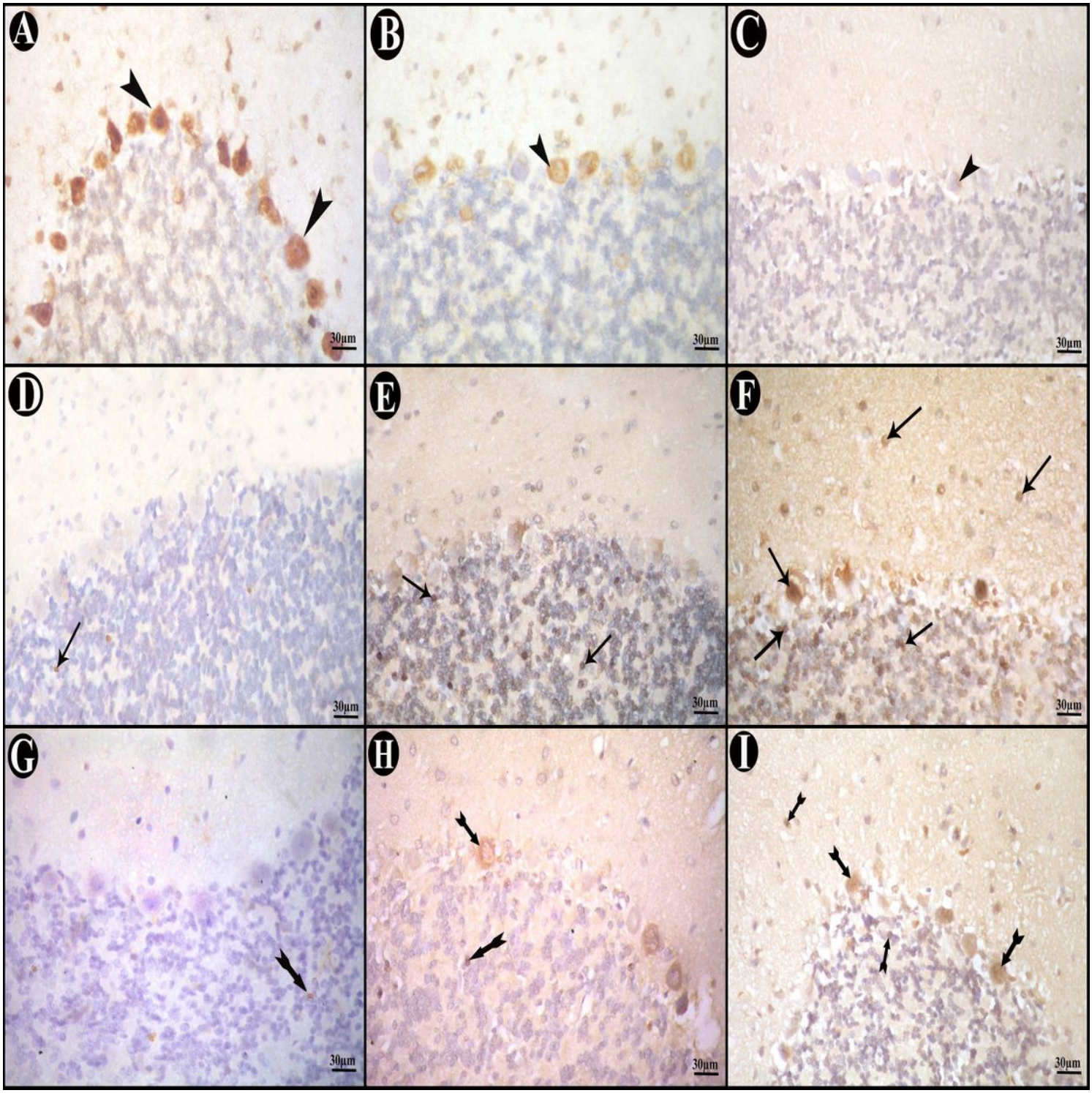

Figure 4

Immunohistochemically stained sections in cerebellar cortex of the study groups. A, D & G, Control group. B, E & H, Group III. C, F & I, Group IV. A-C, Immune reactions for Calbindin D28k (CB) (arrow head). D-F, c-Jun N-terminal kinase (JNK) immune-reactions (arrows). G-I, Factor kappa beta (NF-κB) immune reactions (tailed arrows).

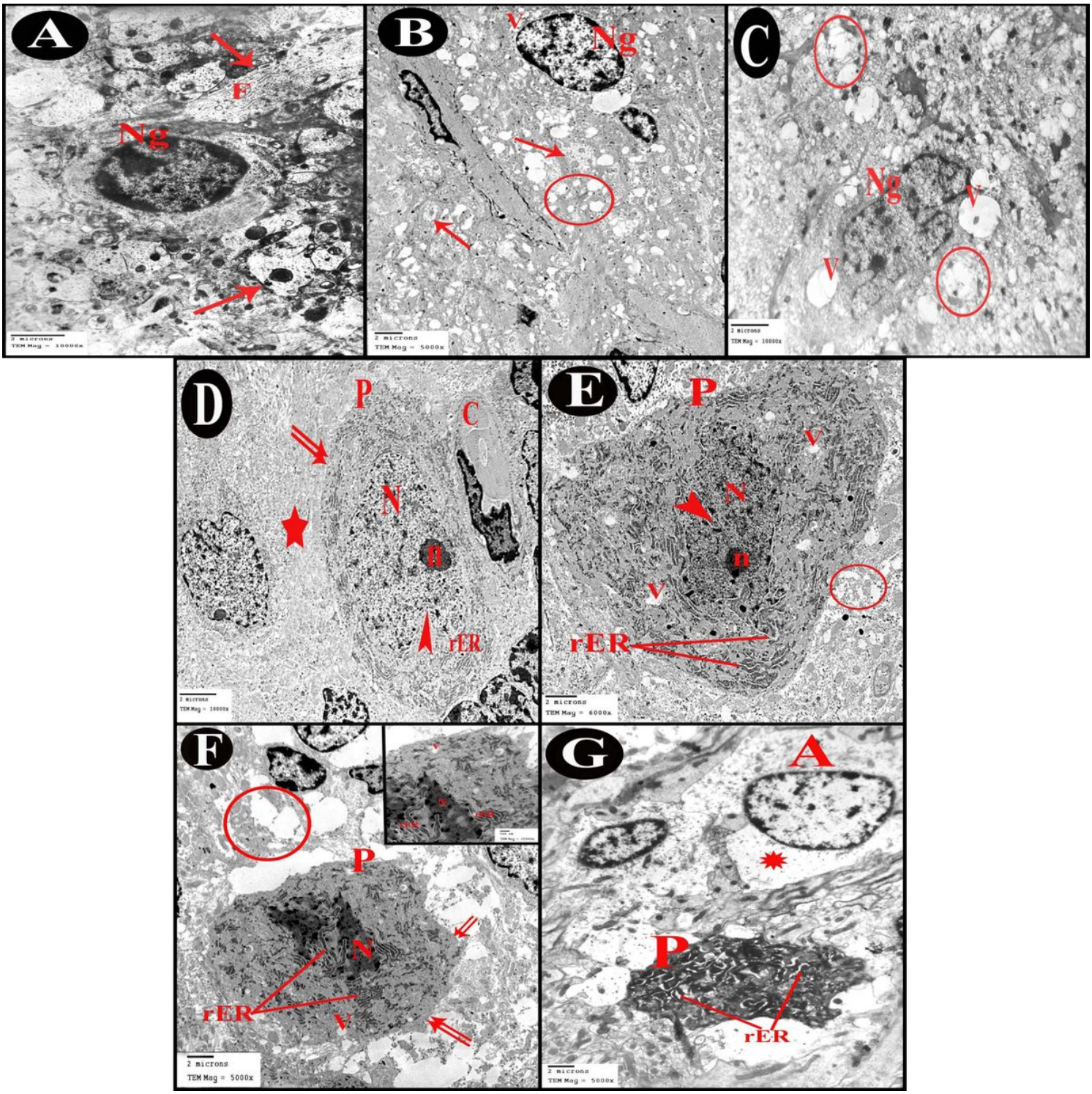

Figure 5

Electron micrographs of rats' cerebellar cortex. A-C molecular layer. A, Control group. B, Group III. C, Group IV. Axons (arrow), neurofilaments (F), neuroglia (Ng), vacuolated neuropil (circle), vacuoles (V). D-G

Purkinje cell layer. D, Control group. E, Group III. F&G, Group IV. Purkinje cell (P), contour of cell membrane (double arrow), tight neuropil (star), blood capillary(C), nucleus (N) with indentation (arrow head), nucleolus (n), short profiles of rough endoplasmic reticulum cisternae (rER), swollen astrocytes (A), loss of cytoplasmic organization (asterix)

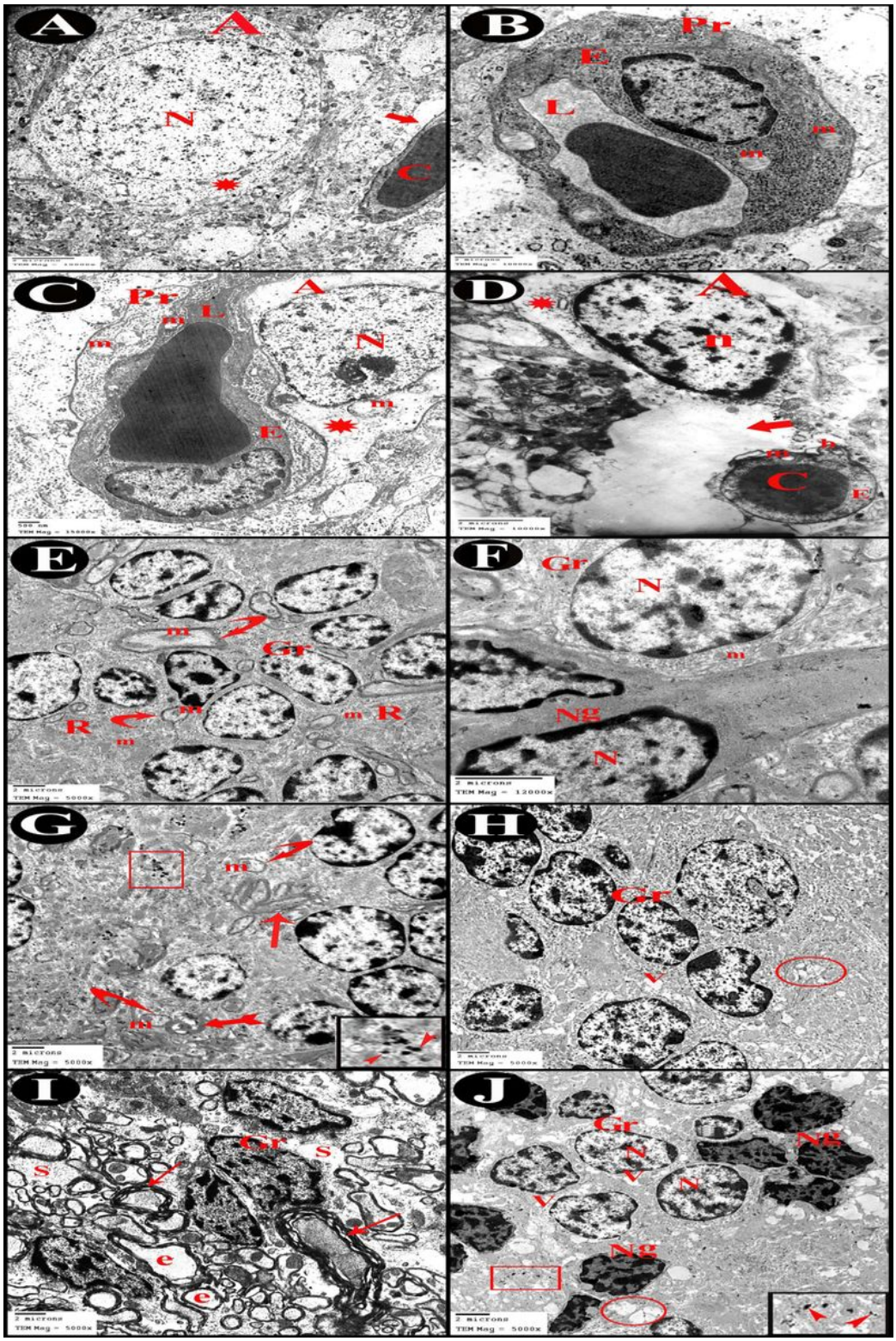

Figure 6

Electron micrographs of rats' cerebellar cortex. A-D, Blood brain barrier. A&B, Control group. C, Group III. D, Group IV. Astrocyte (A), nucleus (N), cytoplasm (asterisk), blood capillary (C) separated by perivascular spaces (thick arrow), lumen of blood capillary (L), endothelial lining (E), mitochondria (m), pericyte cytoplasm (Pr), clumps of heterochromatin within and around the edge of the nucleus (n), separation of the basement membrane (b). E-J, Granular layer. E&F, Control group. G&H, Group III. I&J, Group IV. Granule cells (Gr), mitochondria (m), mossy rosettes (R), neuroglia (Ng), normal myelinated fibers (curved arrow), disrupted myelin (tailed arrow), splitting of myelin sheaths (arrow), vacuoles (V), vacuolated neuropil (circle), ballooned or empty fibers (e), wide spaces between the axons (S). Insets in G&J, magnifications of the boxed parts showing electron dense silver nanoparticles (arrow head).